IEEE Photonics Journal
An IEEE Photonics Society Publication

Open Access

Stochastic Analysis of Miniature Optoelectronic Oscillators Based on Whispering-Gallery Mode Electrooptical Modulators

Volume 13, Number 3, June 2021

Helene Nguewou-Hyousse
Yanne K. Chembo, *Senior Member, IEEE*

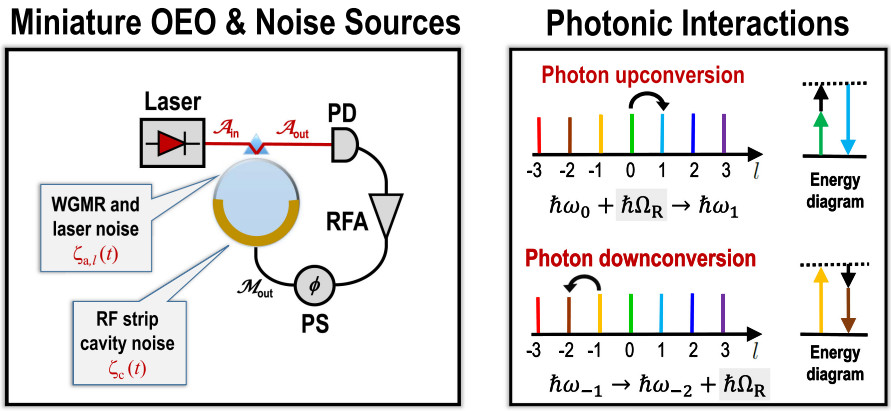

DOI: 10.1109/JPHOT.2021.3070846

Stochastic Analysis of Miniature Optoelectronic Oscillators Based on Whispering-Gallery Mode Electrooptical Modulators

Helene Nguewou-Hyousse and Yanne K. Chembo, *Senior Member, IEEE*

Department of Electrical and Computer Engineering & Institute for Research in Electronics and Applied Physics (IREAP), University of Maryland, College Park, MD 20742 USA

DOI:10.1109/JPHOT.2021.3070846

Manuscript received February 22, 2021; revised March 22, 2021; accepted March 29, 2021. Date of publication April 5, 2021; date of current version April 26, 2021. This work was supported by the Office of Naval Research (ONR) under the Grant N00014-21-1-2098. Corresponding author: Yanne K.Chembo (e-mail: ykchembo@umd.edu).

Abstract: We propose a theoretical analysis of the stochastic dynamics of miniature optoelectronic oscillators (OEOs) based on whispering-gallery mode resonators. The core element in this microwave photonic oscillator is a high-Q whispering-gallery mode resonator with quadratic nonlinearity, which simultaneously performs electrooptical modulation, frequency filtering and energy storage. This multi-task resonator allows the oscillator to feature improved size, weight and power metrics. In this article, we analyze how the various sources of optical and electrical noise in the oscillator are converted to output microwave signal fluctuations. We use an approach based on stochastic differential equations to characterize the dynamics of the microwave signal as a function of radiofrequency gain and laser pump power. This stochastic analysis also allows us to understand how key parameters of the resonator such as its intrinsic and extrinsic Q-factors influence the system's dynamics below and above threshold. The time-domain numerical simulations for miniature OEO stochastic dynamics provides an excellent agreement with the analytical predictions.

Index Terms: Optoelectronic oscillators, whispering-gallery-mode resonators, phase noise.

1. Introduction

Optoelectronic oscillators (OEOs) have emerged as competitive microwave photonic sources for the generation of ultra-stable radiofrequency signals [1], [2]. In their most simplest architecture, they feature a closed optoelectronic feedback where the nonlinear element is an electrooptical (EO) Mach-Zehnder modulator, the energy storage element is a few-km-long optical delay line, and the frequency-selection element is a radiofrequency filter [3]. Such conventional OEOs have been shown to achieve remarkably high phase noise performances, with a record st to -163 dBc/Hz at 6 kHz offset from a 10 GHz carrier [4].

However, the typical OEO is not optimal from the perspective of size, weight and power (SWAP), mainly because of the km-long fiber delay line. Several OEO architectures have been proposed to improve the SWAP metrics, mainly using whispering-gallery mode (WGM) resonators to replace the fiber spool [5]–[13]. Along that line of research and development, one of the most promising

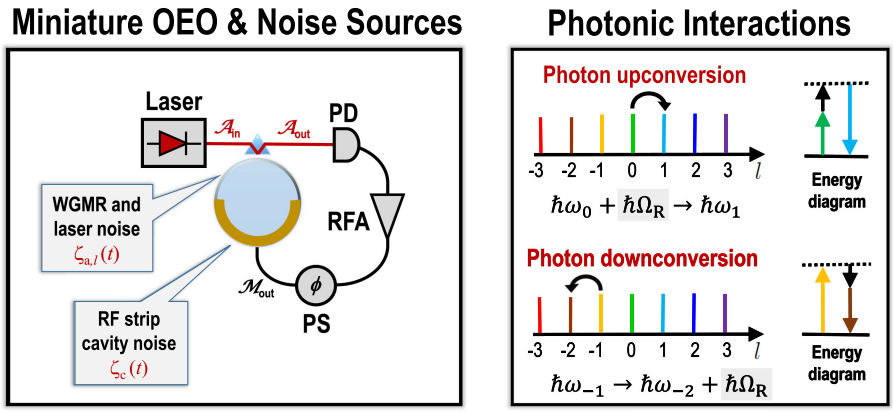

Fig. 1. **Left:** Schematic representation of a miniature OEO, along with the main noise sources. The optical paths are in red, and the electric paths in black. The various sources of noise that ultimately end up driving the stochastic dynamics of the system are explicitly displayed. PD: Photodiode; PS: Phase shifter; RFA: RF amplifier; WGMR: Whispering-gallery mode resonator. **Right:** Frequency-domain representation of photonic conversion processes in the WGMR, mediated by the $g \propto \chi^{(2)}$ nonlinearity. For photonic upconversion an infrared photon annihilates a microwave photon and is upconverted as $\hbar\omega_l + \hbar\Omega_R \rightarrow \hbar\omega_{l+1}$. For photonic downconversion, an infrared photon emits a microwave photon and is downconverted as $\hbar\omega_l \rightarrow \hbar\omega_{l-1} + \hbar\Omega_R$.

architecture is the miniature OEO, where the WGM resonator simultaneously performs electrooptical modulation, frequency filtering and energy storage. As a consequence, the WGM resonator single-handedly replaces the integrated electrooptical Mach-Zehnder modulator, the microwave radiofrequency filter, and the fiber delay line, thereby leading to a drastic improvement of the SWAP metrics.

In miniature OEOs, the electric-to-optical conversion in the WGM modulator is mediated by the quadratic bulk nonlinearity of the resonator [14]–[16]. This deterministic process, which is dynamically complex and high-dimensional, is today well understood [17]. However, there is no analysis available to understand how the optical and electrical noise sources in the optoelectronic loop are converted into microwave phase noise. Such an analysis is indispensable to gain a deep understanding of the metrological performances of this oscillator. In this article, we propose to use a methodology based on stochastic differential equations to achieve this goal. The main idea of this theory (also known as "Langevin" approach) is to add random noise terms to the core deterministic model, and to monitor how these fluctuations are driving the variables of interest – here the phase noise of the output microwave. This approach has already been used with remarkable success for fiber-based OEOs, where it was shown that it can provide an excellent agreement with experimental phase noise spectra [18]–[21].

This article is organized as follows. In Section 2, we describe the miniature OEO under study, as well as the deterministic model that rules its nonlinear temporal dynamics. Section III is devoted to the derivation of the stochastic model, with an emphasis on sources of noise originating from the resonant WGM/RF cavities and from the active electronic elements (photodiode and amplifier). The dynamics of the system under threshold is investigated in Sec. IV, while Sec. V presents a stochastic normal form approach that allows us to analyze the effect of noise below and above threshold. The last section concludes the article.

2. System and Deterministic Model

The schematic representation of the miniature OEO under study is displayed in Fig. 1. The core element of this oscillator is a whispering-gallery mode resonator (see refs. [22]–[26] for a detailed description of their linear and nonlinear properties). In our system, the WGM disk-resonator is

made with a lithium niobate (LN) and it plays the role of a resonant electrooptical modulator. It has a radius a and free spectral range $\Omega_R = c/an_g$, where n_g is the group velocity index at the pump wavelength, and c is the velocity of light in vacuum. The WGM cavity has a loaded quality factor $Q = \omega_L/2\kappa$, where $\kappa = \kappa_i + \kappa_e$ is the loaded half-linewidth of the resonances, while κ_i and κ_e are the intrinsic and extrinsic (i.e., coupling) contributions, respectively. The optical input of this modulator is a telecom laser signal at power P_L with wavelength $\lambda_L \simeq 1550$ nm and angular frequency is $\omega_L = 2\pi c/\lambda_L$. The pumped WGM has an azimuthal order ℓ_0, and will nonlinearly interact with the adjacent modes of the same family ($\ell = \ell_0, \ell_0 \pm 1, \ell_0 \pm 2$). We conveniently introduce the reduced azimuthal order $l = \ell - \ell_0$ so that the WGMs of interest are now symmetrically labeled as $l = 0, \pm1, \pm2, \cdots$, with $l = 0$ being the pumped mode. The fundamental methodology to describe WGM resonators can be found in refs. [26]. The RF strip resonator coupled to the WGM disk has a resonance frequency matching the FSR of the WGM cavity, with a loaded quality factor $Q_M = \Omega_R/2\mu$, with μ being the half-linewidth of the loaded RF cavity resonance (and analogously to the optical case, the intrinsic and extrinsic contributions are μ_i and μ_e, respectively). The coherent interaction between the microwave photons $\hbar\Omega_M$ fed to the RF strip cavity and the optical photons $\hbar\omega_l$ circulating inside the WGM cavity is mediated by a coupling parameter $g \propto \chi^{(2)}$. At the photon level, this interaction leads to parametric upconversion following $\hbar\omega_l + \hbar\Omega_R \rightarrow \hbar\omega_{l+1}$, or to parametric downconversion following $\hbar\omega_l \rightarrow \hbar\omega_{l-1} + \hbar\Omega_R$. These parametric conversion phenomena permit the realization of compact WGM modulators [27]–[31] and ultra-sensitive microwave photonic receivers [32]–[40].

The multimode optical signal exiting the WGM resonator is sent to a photodetector with sensitivity S (in units of V/W), which retrieves the intermodal microwave frequency, and feed it back to the RF electrode of the WGM electrooptical modulator (input impedance R_{out}) after amplification and eventually a phase-shift.

The variables of interest for the oscillator are the complex-valued modal optical amplitudes $\mathcal{A}_l(t)$ of carrier frequency $\omega_L + l\Omega_R$ (normalized such that $|\mathcal{A}_l|^2$ is the number of optical photons in the mode l) and the amplitude of the complex-valued microwave field in the RF cavity $\mathcal{C}(t)$ of carrier frequency Ω_R (normalized such that $|\mathcal{C}|^2$ is the number of microwave photons in the strip). These dimensionless intracavity fields obey the following set of coupled equations [17]:

$$\dot{\mathcal{A}}_l = -\kappa(1+i\alpha)\mathcal{A}_l - ig[\mathcal{C}\mathcal{A}_{l-1} + \mathcal{C}^*\mathcal{A}_{l+1}] + \delta(l)\sqrt{2\kappa_e}\,A_{in} \tag{1}$$

$$\dot{\mathcal{C}} = -\mu(1+i\vartheta)\mathcal{C} - ig\sum_m \mathcal{A}_m^*\mathcal{A}_{m+1} + \Gamma e^{i\Phi}\,\eta\left\{2\kappa_e\sum_m \mathcal{A}_m^*\mathcal{A}_{m+1} - A_{in}\sqrt{2\kappa_e}(\mathcal{A}_{-1}^* + \mathcal{A}_1)\right\}, \tag{2}$$

where $\delta(l)$ is the Kronecker function (equal to 1 for $l = 0$ and to zero otherwise), the dimensionless constant $\eta = 2\hbar\omega_L S\sqrt{\mu_e/R_{out}\hbar\Omega_R}$ is a characteristic optoelectronic parameter of the oscillator, Φ is the microwave rountrip phase shift, $\alpha = -(\omega_L - \omega_0)/\kappa$ is the normalized optical detuning between the laser and the pumped mode resonance, and $\vartheta = -(\Omega_M - \Omega_R)/\mu$, is the normalized detuning between the RF signal and the strip cavity resonance (set to 0 in this study). A key parameter of the oscillator is the real-valued dimensionless feedback gain $\Gamma = G_A G_L \geq 0$ where where G_A (> 1) is the RF amplifier gain while G_L (< 1) is the overall loss factor of the electric branch. The laser pump field of the WGM resonator is $A_{in} = \sqrt{P_L/\hbar\omega_L}$: It is a real-valued envelope (null phase), and for that reason it plays the role of reference for all the intracavity fields $\mathcal{A}_l$.

The overall optical field exiting the WGM resonator is $\mathcal{A}_{out} = \sum_l \mathcal{A}_{out,l}\, e^{il\Omega_R t}$, with $\mathcal{A}_{out,l} = -A_{in}\,\delta(l) + \sqrt{2\kappa_e}\,\mathcal{A}_l$ being the modal output fields [Note that they are propagating field like A_{in} and their square modulus is therefore also a photon flux in units of s^{-1}]. An infinite-bandwidth photodetector would output a RF signal proportional to the incoming optical power following $V_{PD}(t) = SP_{opt,out} = \hbar\omega_L S|\mathcal{A}_{out}|^2$ (in volts), which can be Fourier-expanded as:

$$V_{PD}(t) = \frac{1}{2}\mathcal{M}_0 + \sum_{n=1}^{+\infty}\left[\frac{1}{2}\mathcal{M}_n\exp(in\Omega_R t) + \text{c.c.}\right] \equiv \sum_{n=0}^{+\infty} V_{PD,n}(t), \quad \text{with } n = 0, 1, 2, \ldots \tag{3}$$

where c.c. stands for the complex conjugate of the preceding terms, and the modal fields

$$\mathcal{M}_n = 2\hbar\omega_{\mathrm{L}}\, S \sum_m \mathcal{A}^*_{\mathrm{out},m}\mathcal{A}_{\mathrm{out},m+n} \tag{4}$$

are the complex-valued envelopes of the microwave harmonics of frequency $n \times \Omega_{\mathrm{R}}$.

The microwave signal of interest is the output of the RF amplifier, which is defined by an envelope $\mathcal{M}_{\mathrm{out}} = \Gamma\mathcal{M}_1 = 2\Gamma\hbar\omega_{\mathrm{L}}\, S \sum_m \mathcal{A}^*_{\mathrm{out},m}\mathcal{A}_{\mathrm{out},m+1}$ and power $P_{\mathrm{rf,out}} = \Gamma^2|\mathcal{M}_1|^2/2R_{\mathrm{out}}$, where R_{out} is the characteristic load resistance in the RF branch.

Previous work has shown that the dynamics of the system described by Eqs. (1) and (2) is strongly dependent on the feedback gain parameter $\Gamma > 0$ [17]. When the feedback gain is below a given critical Γ_{cr}, only the pumped mode $\mathcal{A}_0$ is excited (by the pump laser) and no microwave is generated. However, when $\Gamma > \Gamma_{\mathrm{cr}}$, a cascaded process leads to the excitation of the sidemodes $\mathcal{A}_l$ with $l \neq 0$, thereby leading to the formation of an optical frequency comb that generates a self-sustained microwave oscillation in the electric branch. The analytical value of Γ_{cr} could be determined exactly at the analytical level, even though the related formula appeared to be mathematically quite involved. However, in the limit $\kappa/\mu \ll 1$ (optical resonances are much narrower than microwave ones), the critical gain could be explicitly expressed as

$$\Gamma_{\mathrm{cr}} \simeq \frac{1}{\rho(1-\rho)}\,\frac{1+\alpha^2}{2|\alpha|}\,\frac{\mu\kappa_{\mathrm{i}}}{g\eta P_{\mathrm{L}}}\,\hbar\omega_{\mathrm{L}}\,, \tag{5}$$

where $\rho = \kappa_{\mathrm{e}}/\kappa \in [0, 1]$ is the ratio between outcoupling and total losses in the resonator – we have undercoupling when $\rho < \frac{1}{2}$, overcoupling when $\rho < \frac{1}{2}$, and critical coupling when $\rho = \frac{1}{2}$. The first two terms in Eq. (5) indicates that Γ_{cr} is minimized by critical coupling and edge-of-resonance detuning ($\alpha = \pm 1$), respectively. The same stability for the system also indicated that the roundtrip Φ phase shift has to be set to 0 when $\alpha > 0$, and to π when $\alpha < 0$ [as inferred in Eq. (5), null optical detuning should be avoided as it leads to prohibitively large critical gain values].

Unless otherwise stated, we will consider the following parameters for our system throughout this article, without loss of generality: $P_{\mathrm{L}} = 1$ mW; $\lambda_{\mathrm{L}} = 1550$ nm; $\Omega_{\mathrm{R}}/2\pi = 10$ GHz; $S = 20$ V/W; $g/2\pi = 20$ Hz; $Q_{\mathrm{i}} = 5 \times 10^7$ and $Q_{\mathrm{e}} = 10^7$ (this defines all the κ coefficients); $Q_{\mathrm{M}} = \Omega_{\mathrm{R}}/2\mu = 100$; and finally, the RF line is impedance-matched with the modulator input electrode with $R_{\mathrm{out}} = 50\ \Omega$ and $\mu_{\mathrm{i}} = \mu_{\mathrm{e}} = \mu/2$.

3. Noise Sources and Stochastic Model for the Miniature OEO

The object of this section is to identify the most relevant sources of noise in the oscillator, and define how they should be accounted for in the stochastic model. These random noise terms either have an additive or multiplicative effect on the system's dynamics. However, in this work, we will only focus on the additive noise source terms, which in our context are dominant. Moreover, for the sake of simplicity, these random noise signals will be assumed to be Gaussian and white. Therefore, depending on their real- or complex-valued nature, these random signals will always be proportional to either a real-valued Gaussian white noise $\xi(t)$ with $\langle\xi(t)\xi(t')\rangle = \delta(t-t')$, or to a complex-valued Gaussian white noise $\zeta(t)$ with $\langle\zeta(t)\zeta^*(t')\rangle = \delta(t-t')$.

The miniature OEO has two cavities (optical WGM resonator and RF strip resonator), which are driven by external optical and radiofrequency signals, respectively. Indeed, the oscillator is unavoidably submitted to the influence of various random noise sources, which end up driving the stochastic fluctuations of the intracavity fields. The optical fields $\mathcal{A}_l(t)$ are driven by a modal random field normalized as $\Lambda_{\mathrm{a}}\sqrt{2\kappa}\,\zeta_{\mathrm{a},l}(t)$, which has to be added in the right-hand side of Eq. (1). One should note that this noise term will create Λ_{a}^2 optical photons on average in each mode l [17], [41]. Analogously, The intracavity microwave field $\mathcal{C}(t)$ is driven by a random signal normalized as $\Lambda_{\mathrm{c}}\sqrt{2\mu}\,\zeta_{\mathrm{c}}(t)$ to be added in the right-hand side of Eq. (2), that will generate Λ_{c}^2 microwave photons on average inside the RF strip cavity.

The sources of noise in the miniature OEO can now be added to the core deterministic Eqs. (1) and (2) to obtain the following stochastic model:

$$\dot{\mathcal{A}}_l = -\kappa(1+i\alpha)\mathcal{A}_l - ig[\mathcal{C}\mathcal{A}_{l-1} + \mathcal{C}^*\mathcal{A}_{l+1}] + \delta(l)\sqrt{2\kappa_e}\,A_{\text{in}} + \Lambda_a\sqrt{2\kappa}\,\zeta_{a,l}(t) \tag{6}$$

$$\dot{\mathcal{C}} = -\mu(1+i\vartheta)\mathcal{C} - ig\sum_m \mathcal{A}_m^*\mathcal{A}_{m+1} + \Gamma e^{i\Phi}\eta\left\{+2\kappa_e\sum_m \mathcal{A}_m^*\mathcal{A}_{m+1} - A_{\text{in}}\sqrt{2\kappa_e}(\mathcal{A}_{-1}^* + \mathcal{A}_1)\right\} + \Lambda_c\sqrt{2\mu}\,\zeta_c(t)\,, \tag{7}$$

with the noise correlations $\langle\zeta_{a,l}(t)\zeta_{a,l'}^*(t')\rangle = \delta_{l,l'}\delta(t-t')$ and $\langle\zeta_c(t)\zeta_c^*(t')\rangle = \delta(t-t')$. The noisy output microwave signal is still $\mathcal{M}_{\text{out}}(t) = \Gamma e^{i\Phi}\mathcal{M}_1(t)$ and the output RF power is still determined by $P_{\text{rf,out}} = |\mathcal{M}_{\text{out}}|^2/2R_{\text{out}} = \Gamma^2|\mathcal{M}_1|^2/2R_{\text{out}}$. One can note that when the sources of noise are discarded, the stochastic Eqs. (6) and (7) degenerate into the deterministic Eqs. (1) and (2). In this article, the stochastic differential Eqs. (6) and (7) will be numerically simulated using the Milstein algorithm (see ref. [42]).

4. Stochastic Analysis Under Threshold

In this section, we aim at calculating the microwave power generated under threshold, that is, when $\Gamma < \Gamma_{\text{cr}}$. The sub-threshold dynamics is generally overlooked in the literature, but however, previous studies have shown that the sub-threshold stochastic dynamics is important in order to characterize the various sources of noise in the system (see for example ref. [18]).

The microwave power generated under threshold can be obtained via the numerical simulation of Eqs. (6) and (7), whose output can be suitably averaged to give

$$P_{\text{rf,out}} = \frac{1}{2R_{\text{out}}}\langle|\mathcal{M}_{\text{out}}(t)|^2\rangle = \frac{\Gamma^2}{2R_{\text{out}}}\langle|\mathcal{M}_1(t)|^2\rangle\,. \tag{8}$$

However, these numerical simulations do not give any theoretical insight into why the subthreshold noise increases the way it does with the gain. In the case of the miniature OEO under threshold, it is possible to develop an analytical method to achieve this goal. The starting point is to note that the stochastic model displayed in Eqs. (6) and (7) can be simplified using two assumptions. The first one is that stochastic effects in the intracavity fields $\mathcal{A}_l$ and $\mathcal{C}$ can be accounted for via the output microwave field $\mathcal{M}_1$. The second one is that below threshold, there is no self-sustained microwave oscillation and as a consequence, only the mode $l = 0$ is excited with $\mathcal{A}_0 = \sqrt{2\kappa_e}A_{\text{in}}/\kappa(1+i\alpha)$. The intracavity fields $\mathcal{A}_{\pm1}$ and $\mathcal{C}$ are of first order of smallness and can be linearized around zero, while the fields $\mathcal{A}_l$ with $|l| > 1$ can be outright neglected for being of higher order of smallness.

Using these two simplifying assumptions, the stochastic Eqs. (6) and (7) are now reduced to

$$\delta\dot{\mathcal{A}}_{-1}^* = -\kappa(1-i\alpha)\delta\mathcal{A}_{-1}^* + ig\mathcal{A}_0^*\delta\mathcal{C} + \Lambda_a\sqrt{2\kappa}\,\zeta_{a,-1}(t) \tag{9}$$

$$\delta\dot{\mathcal{A}}_0 = -\kappa(1+i\alpha)\delta\mathcal{A}_0 + \sqrt{2\kappa_e}A_{in} + \Lambda_a\sqrt{2\kappa}\,\zeta_{a,0}(t) \tag{10}$$

$$\delta\dot{\mathcal{A}}_1 = -\kappa(1+i\alpha)\delta\mathcal{A}_1 - ig\mathcal{A}_0\delta\mathcal{C} + \Lambda_a\sqrt{2\kappa}\,\zeta_{a,1}(t) \tag{11}$$

$$\delta\dot{\mathcal{C}} = -\mu(1+i\vartheta)\delta\mathcal{C} - ig[\mathcal{A}_0\delta\mathcal{A}_{-1}^* + \mathcal{A}_0^*\delta\mathcal{A}_1] + \beta\left\{2\kappa_e[\mathcal{A}_0\delta\mathcal{A}_{-1}^* + \mathcal{A}_0^*\delta\mathcal{A}_1] - \sqrt{2\kappa_e}A_{\text{in}}(\delta\mathcal{A}_{-1}^* + \delta\mathcal{A}_1)\right\} + \Lambda_c\sqrt{2\mu}\,\zeta_c(t) \tag{12}$$

where $\beta = \eta\Gamma e^{i\Phi}$ is the overall electrical gain of the OEO. The perturbation $\delta\mathcal{A}_0$ is independent of the other ones and is irrelevant in the subsequent analysis for being permanently dominated by the non-null amplitude $\mathcal{A}_0$. Therefore, we can ignore the corresponding equation and rewrite the

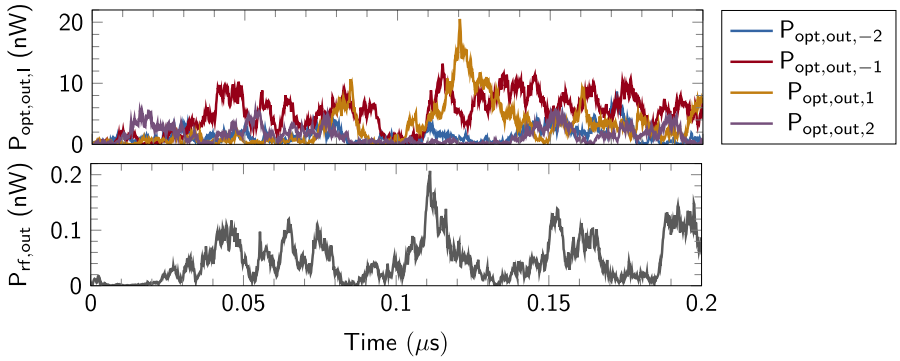

Fig. 2. Temporal variation of the optical and microwave output noise powers when the feedback gain is set to $\Gamma = 6$ (or $\gamma = \Gamma/\Gamma_{cr} = 0.54$) and $\Lambda_{a,c} = 10$. The numerical results are obtained via the time-domain simulation of the stochastic differential Eqs. (6) and (7). **Top**: Temporal dynamics of $P_{opt,out,l} = \hbar\omega_L |\mathcal{A}_{out,l}|^2$; **Bottom**: Temporal dynamics of $P_{rf,out}$.

remaining three linear equations in the Fourier domain to obtain

$$\begin{bmatrix} \delta\tilde{\mathcal{A}}^*_{-1}(\omega) \\ \delta\tilde{\mathcal{A}}_1(\omega) \\ \delta\tilde{\mathcal{C}}(\omega) \end{bmatrix} = \Big[i\omega \mathbf{I}_3 - \mathbf{J} \Big]^{-1} \begin{bmatrix} \Lambda_a\sqrt{2\kappa}\, \tilde{\mathcal{Z}}^*_{a,-1}(\omega) \\ \Lambda_a\sqrt{2\kappa}\, \tilde{\mathcal{Z}}_{a,1}(\omega) \\ \Lambda_c\sqrt{2\mu}\, \tilde{\mathcal{Z}}_c(\omega) \end{bmatrix}, \tag{13}$$

where $\mathbf{I}_3$ is the three-dimensional identity matrix and

$$\mathbf{J} = \begin{bmatrix} -\kappa(1 - i\alpha) & 0 & ig\mathcal{A}^*_0 \\ 0 & -\kappa(1 + i\alpha) & -ig\mathcal{A}_0 \\ \sqrt{2\kappa_e}\beta\mathcal{A}_{out,0} - ig\mathcal{A}_0 & \sqrt{2\kappa_e}\beta\mathcal{A}^*_{out,0} - ig\mathcal{A}^*_0 & -\mu(1 + i\vartheta) \end{bmatrix} \tag{14}$$

is the Jacobian of the linear flow, with the variables $\tilde{\mathcal{Z}}(\omega)$ being the Fourier transform of their stochastic counterparts $\zeta(t)$. In the Fourier domain, Eq. (14) permits to determine *explicitly* the three stochastic variables of interest as a linear combination of the intracavity noise terms $\tilde{\mathcal{Z}}_{a,c}(\omega)$. In principle, the time-domain solutions could be recovered via an inverse Fourier transform.

Using Eq. (4), it appears that the output microwave signal $\mathcal{M}_1(t)$ is now a linear combination of $\delta\mathcal{A}_1(t)$ and $\delta\mathcal{A}^*_{-1}(t)$. This linearity can be translated in the Fourier domain following

$$\tilde{\mathcal{M}}_1(\omega) = 2\hbar\omega_L S\sqrt{2\kappa_e}\left\{\mathcal{A}_{out,0}\delta\tilde{\mathcal{A}}^*_{-1}(\omega) + \mathcal{A}^*_{out,0}\delta\tilde{\mathcal{A}}_1(\omega)\right\}, \tag{15}$$

which implies that $\tilde{\mathcal{M}}_1(\omega)$ is also a linear combination of the intracavity noise terms $\tilde{\mathcal{Z}}_{a,c}(\omega)$.

We can now define the sub-threshold microwave output power after the RF amplifier as

$$P_{rf,out} = \frac{\Gamma^2}{2R_{out}}\left\{\frac{1}{2\pi}\int_{-\infty}^{+\infty} |\tilde{\mathcal{M}}_1(\omega)|^2\, d\omega\right\}, \tag{16}$$

where we are using Parseval's theorem since we explicitly know $\tilde{\mathcal{M}}_1(\omega)$ via Eq. (15).

Figure 2 displays the modal power dynamics as a function of time for the four centermost side-modes, for a given value of the feedback gain. On the other hand, Fig. 3 displays the comparison between the analytical formula of Eq. (16) and the numerical simulations using Eq. (8) via the time-domain stochastic differential Eqs. (6) and (7). The normalized gain $\gamma \equiv \Gamma/\Gamma_{cr}$ is increased under threshold ($\gamma < 1$) and the variation of the noise power $P_{rf,out} = |\mathcal{M}_{out}|^2/2R_{out}$ is determined for various values of the noise amplitudes $\Lambda_{a,c}$. One can note that the analytical formula predicts accurately the growth of noise power as the gain is increased, thereby confirming the validity of the theoretical approach.

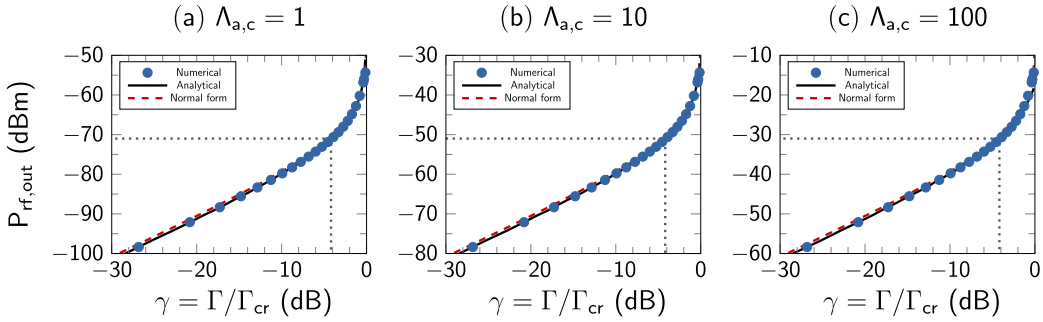

Fig. 3. Variation of the noise power $P_{rf,out} = |\mathcal{M}_{out}|^2/2R_{out}$, when the normalized gain $\gamma \equiv \Gamma/\Gamma_{cr}$ is increased under threshold. We have $\gamma < 1$, so that the gain in dB is 20 $\log\gamma$, and is negative. The plots from left to right correspond to noise amplitudes $\Lambda_{a,c} = 1$, 10, and 100 respectively. The blue dot symbols stand for the numerical results obtained using Eq. (8), via the time-domain simulation of the stochastic differential Eqs. (6) and (7). The continuous black lines stand for analytical results obtained via Eq. (16). The dashed red lines stand for the scaling behavior as predicted by the normal form theory in Eq. (20). The dotted gray lines indicate the microwave noise power corresponding to a gain of -4.18 dB, which directly gives the amplitude of the driving Gaussian white noise power in the normal form model (from left to right, $p_{out} = m^2/2R_{out} = -71$, -51, and -31 dBm, respectively). One can note the excellent agreement between numerical simulations and analytical predictions.

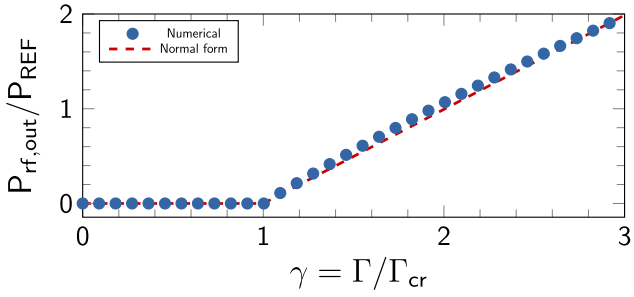

Fig. 4. Variation of the microwave power $P_{rf,out} = |\mathcal{M}_{out}|^2/2R_{out}$, when the normalized gain $\gamma \equiv \Gamma/\Gamma_{cr}$ is increased above threshold ($\gamma > 1$). The blue dot symbols stand for the numerical results obtained using the time-domain simulation of the stochastic differential Eqs. (6) and (7). The dashed red lines stand for the scaling behavior as predicted by the normal form theory in Eq. (18). The microwave power has been normalized to an arbitrary reference power P_{REF} in order to evidence the scaling $\propto \gamma - 1$ above threshold predicted by Eq. (18) for $P_{rf,out} \propto |\mathcal{M}|^2$. One can note the good agreement between numerical simulations and analytical predictions. The linear scaling of the power with the gain above threshold is expected to break down when $\gamma \gg 1$ because of the higher-order nonlinear terms neglected in the normal form approach are then becoming dominant.

5. Normal Form Approach for Stochastic Analysis and Phase Noise

The deterministic dynamics of the miniature OEO as described in Eqs. (1) and (2) is high-dimensional and non-trivial. For example, it was shown in ref. [17] that above threshold, symmetric modes with eigenumbers $\pm l$ do not have the same amplitude, and are therefore beyond any tractable analytical approximation. However, the microwave signal is only two-dimensional (complex-valued envelope carrying information about amplitude and phase), and certainly more amenable to mathematical analysis across a gain range covering the regimes below and above threshold. Moreover, having a differential equation for the microwave variable would enable us to investigate analytically its phase noise properties.

One could try to obtain an exact equation for $\dot{\mathcal{M}}_1$ through the time derivation of Eq. (4). This operation would result in expressing $\dot{\mathcal{M}}_1$ as a nonlinear expansion of terms $\dot{\mathcal{A}}_l^* \mathcal{A}_{l+1}$ and $\mathcal{A}_l^* \dot{\mathcal{A}}_{l+1}$, but would not yield a closed-form differential equation that only depends on $\mathcal{M}_1$. However, from the

nonlinear dynamics systems point of view, the onset of the microwave oscillation can be viewed as the result of a Hopf bifurcation. As a consequence, normal form theory states that there is a closed-form equation for the microwave valid at least close to the vicinity of the bifurcation, with arbitrarily high precision. The bifurcation will be characterized by a linear parameter a, and a nonlinear parameter b.

In general, a large (but finite) sequence of involved mathematical operations are needed to determine the parameters a and b, even for low-dimensional systems (see for example ref. [43]). In our case, the minimum number of optical modes considered above threshold is 11 (with l varying from -5 to 5), so that Eqs. (1) and (2) are *at least* 24-dimensional: Under these conditions, following the standard mathematical protocol to derive the normal form coefficients is practically difficult to carry out. However, we will show that in the stochastic regime, using the normal form approach will provide the scaling behaviors of interest below and above threshold.

In this study, we will write the *stochastic* normal form equation for the microwave as

$$\dot{\mathcal{M}} = -a\mathcal{M} + \gamma[a\mathcal{M} + m\sqrt{2a}\,\zeta_{\mathrm{m}}(t)] - ab|\mathcal{M}|^2\mathcal{M}\,, \tag{17}$$

where $\mathcal{M} = |\mathcal{M}|e^{i\psi} \propto \mathcal{M}_{\mathrm{out}}$ is the complex-valued microwave envelope of interest (in V), a stands for the linear damping of the microwave (in rad/s), b stands for the nonlinear saturation (in V^{-2}), m stands for the root-mean-square amplitude (in V) of the driving Gaussian white noise, which is delta-correlated as $\langle\zeta_{\mathrm{m}}(t)\zeta_{\mathrm{m}}^*(t')\rangle = \delta(t-t')$. The parameter $\gamma \equiv \Gamma/\Gamma_{\mathrm{cr}} > 0$ is the normalized feedback gain, which is here affecting both the microwave and the random noise.

In its deterministic version ($m = 0$), the normal form in Eq. (17) yields the following solution:

$$|\mathcal{M}| = \begin{cases} 0 & \text{when } \gamma < 1 \\ \sqrt{(\gamma-1)/b} \equiv M_b\sqrt{\gamma-1} & \text{when } \gamma > 1 \end{cases}, \tag{18}$$

where $M_b = 1/\sqrt{b}$ can be interpreted as the characteristic amplitude of $\mathcal{M}$ (in V). In other words, the trivial solution is stable when $\gamma < 1$, while the nontrivial (i.e. oscillatory) solution is stable when $\gamma > 1$. However, when noise is accounted for, the stochastic behavior deviates substantially from the deterministic one.

In the stochastic sub-threshold case ($m \neq 0$ and $\gamma < 1$), the linear terms are of first order of smallness, while the nonlinear term is of third order of smallness and can then be neglected. Equation (17) is therefore reduced to the well-known Ornstein-Uhlenbeck process, whose stationary properties can be obtained analytically. We first rewrite Eq. (17) in the Fourier domain as

$$\tilde{\mathcal{M}}(\omega) = \frac{\gamma m\sqrt{2a}}{(1-\gamma)a + i\omega}\,\tilde{\mathcal{Z}}_{\mathrm{m}}(\omega) \tag{19}$$

from which we calculate the corresponding power using again Parseval's theorem, leading to

$$P_{\mathrm{rf,out}} = \frac{1}{2R_{\mathrm{out}}}\langle|\mathcal{M}(t)|^2\rangle = \frac{1}{2R_{\mathrm{out}}}\left\{\frac{1}{2\pi}\int_{-\infty}^{+\infty}|\tilde{\mathcal{M}}(\omega)|^2\,d\omega\right\} = \frac{\gamma^2}{1-\gamma}\,\frac{m^2}{2R_{\mathrm{out}}}\,. \tag{20}$$

It appears that the microwave power under threshold should distinctively scale as $\gamma^2/(1-\gamma)$, and the coefficient of proportionality is the noise power $p_{\mathrm{out}} = m^2/2R_{\mathrm{out}}$. Interestingly, $P_{\mathrm{rf,out}} = p_{\mathrm{out}}$ (i.e., the power of the output signal and input noise are equal) when $\gamma^2 = 1-\gamma$, that is, when $\gamma = (\sqrt{5}-1)/2 \simeq 0.618$ (or -4.18 dB). This property is useful in order to retrieve the parameter m via p_{out} from the sub-threshold power variation as a function of gain. Figure 3 displays the comparison between the numerical simulations using Eq. (8) and the scaling law predicted by the normal form theory in Eq. (20). The excellent agreement confirms the validity of the scaling behavior predicted by the normal form theory.

The stochastic dynamics above threshold corresponds to $m \neq 0$ and $\gamma > 1$. In this case, it is customary to neglect amplitude noise in comparison to phase noise [$\partial_t|\mathcal{M}| \simeq 0$], so that the amplitude of the microwave is still considered constant and given by Eq. (18). As a consequence,

the stochastic Eq. (17) is reduced to

$$\dot{\mathcal{M}} = [\partial_t|\mathcal{M}| + i\dot{\psi}|\mathcal{M}|]\, e^{i\psi} \simeq i\dot{\psi}|\mathcal{M}|\, e^{i\psi}$$
$$\simeq \gamma m\sqrt{2a}\,\zeta_m(t)\,. \tag{21}$$

from which we straightforwardly derive the phase noise spectrum as

$$|\tilde{\Psi}(\omega)|^2 = \frac{1}{\omega^2}\left[\frac{a\gamma^2 m^2}{|\mathcal{M}|^2}\right] \simeq \frac{\gamma^2}{\gamma-1}\,\frac{ab\,m^2}{\omega^2} \tag{22}$$

in units of rad^2/Hz. This phase noise spectrum displays the usual f^{-2} dependence for oscillators driven by white noise, and the normal form analysis provides two key elements for phase noise optimization. The first one is that the diffusion coefficient of the phase noise is $D = abm^2$: In other words, it depends on the three parameters that characterize the stochastic normal form Eq. (17). From the physical viewpoint, we find as expected that the phase noise is reduced by lower cavity losses ($a \to 0$) and lower driving noise ($m^2 \to 0$). The intuition that larger microwave signals improve the phase noise performance is recovered from the condition $b \to 0$, which corresponds to a large *characteristic* voltage for the oscillator. The second one is that since phase noise scales as $\gamma^2/(\gamma-1)$, increasing the gain leads to a deterioration of the phase noise performance by a factor $\sim\gamma$ when $\gamma \gg 1$. Therefore, increasing the microwave signal to decrease phase noise via a larger γ will not be successful for miniature OEOs – instead, as indicated above, large signals should be obtained by design with the lowest b possible.

6. Conclusion

In this article, we have investigated the stochastic dynamics of an architecture of miniature OEO. We have first introduced the stochastic differential equations ruling the dynamics of the system when driven by white noise sources, and provided an analytical framework to determine the power of the generated microwave. We have also proposed a stochastic normal form approach to extract the scaling behavior of the microwave power as the gain is increased below and above threshold. The analytical results were found to be in excellent agreement with the numerical simulations. Future work will be devoted to the development of a more complete model that will account for other nonlinear effects in the resonators or optoelectronic components of the feedback loop, and the model will be extended to account for multiplicative and $1/f$ noise.

References

[1] L. Maleki, "The optoelectronic oscillator," *Nature Phot.*, vol. 5, pp. 728–730, 2011.
[2] Y. K. Chembo, D. Brunner, M. Jacquot, and L. Larger, "Optoelectronic oscillators with time-delayed feedback," *Rev. Mod. Phys.*, vol. 91, 2019, Art. no. 035006.
[3] X. S. Yao and L. Maleki, "High frequency optical subcarrier generator," *Electron. Lett.*, vol. 30, 1994, Art. no. 1525.
[4] D. Eliyahu, D. Seidel, and L. Maleki, "Phase noise of a high performance OEO and an ultra low noise floor cross-correlation microwave photonic homodyne system," in *Proc. IEEE Int. Freq. Control Symp.*, 2008, pp. 811–814.
[5] K. Volyanskiy, P. Salzenstein, H. Tavernier, M. Pogurmirskiy, Y. K. Chembo, and L. Larger, "Compact optoelectronic microwave oscillators using ultra-high Qwhispering gallery mode disk-resonators and phase modulation," *Opt. Exp.* vol. 18, 2010, Art. no. 22358.
[6] P.-H. Merrer, K. Saleh, O. Llopis, S. Berneschi, F. Cosi, and G. Nunzi Conti, "Characterization technique of optical whispering gallery mode resonators in the microwave frequency domain for optoelectronic oscillators," *Appl. Opt.*, vol. 51, 2012, Art. no. 4742.
[7] D. Eliyahu *et al.*, "Resonant widely tunable opto-electronic oscillator," *IEEE Photon. Technol. Lett.*, vol. 25, no. 15, pp. 1535–1538, Aug. 2013.
[8] A. Coillet, R. Henriet, P. Salzenstein, K. P. Huy, L. Larger, and Y. K. Chembo, "Time-domain dynamics and stability analysis of optoelectronic oscillators based on whispering-gallery mode resonators," *IEEE J. Sel. Topics Quantum Electron.*, vol. 19, no. 5, pp. 1–12, Sep./Oct. 2013.
[9] K. Saleh *et al.*, "Phase noise performance comparison between optoelectronic oscillators based on optical delay lines and whispering gallery mode resonators," *Opt. Exp.*, vol. 22, 2014, Art. no. 32158.

[10] K. Saleh, G. Lin, and Y. K. Chembo, "Effect of laser coupling and active stabilization on the phase noise performance of optoelectronic microwave oscillators based on whispering-gallery mode resonators," *IEEE Photon. J.*, vol. 7, no. 1, Feb. 2015, Art. no. 5500111.
[11] K. Saleh and Y. K. Chembo, "Phase noise performance comparison between microwaves generated with kerr optical frequency combs and optoelectronic oscillators," *Electron. Lett.*, vol. 53, 2017, Art. no. 264.
[12] J. Chen, Y. Zheng, C. Xue, C. Zhang, and Y. Chen, "Filtering effect of SiO_2 optical waveguide ring resonator applied to optoelectronic oscillator," *Opt. Exp.*, vol. 26, 2018, Art. no. 12638.
[13] X. Jin, M. Wang, K. Wang, Y. Dong, and L. Yu, "High spectral purity electromagnetically induced transparency-based microwave optoelectronic oscillator with a quasi-cylindrical microcavity," *Opt. Exp.*, vol. 27, 2019, Art. no. 150.
[14] A. B. Matsko, L. Maleki, A. A. Savchenkov, and V. S. Ilchenko, "Whispering gallery mode based optoelectronic microwave oscillator," *J. Mod. Opt.*, vol. 50, 2003, Art. no. 2523.
[15] V. S. Ilchenko, J. Byrd, A. A. Savchenkov, A. B. Matsko, D. Seidel, and L. Maleki, "Miniature oscillators based on optical whispering gallery mode resonators," in *Proc. IEEE Int. Freq. Control Symp.*, 2008, pp. 305–308.
[16] M. Soltani *et al.*, "Ultrahigh Q whispering gallery mode electro-optic resonators on a silicon photonic chip," *Opt. Lett.*, vol. 41, 2016, Art. no. 4375.
[17] H. Nguewou-Hyousse and Y. K. Chembo, "Nonlinear dynamics of miniature optoelectronic oscillators based on whispering-gallery mode electrooptical modulators," *Opt. Exp.*, vol. 28, 2020, Art. no. 30656.
[18] Y. K. Chembo, K. Volyanskiy, L. Larger, E. Rubiola, and P. Colet, "Determination of phase noise spectra in opto-electronic microwave oscillators: A. langevin approach," *IEEE J. Quantum Electron.*, vol. 45, no. 2, pp. 178–186, Feb. 2009.
[19] K. Volyanskiy, Y. K. Chembo, L. Larger, and E. Rubiola, "Contribution of laser frequency and power fluctuations to the microwave phase noise of optoelectronic oscillators," *J. Lightw. Technol.*, vol. 28, no. 18, pp. 2730–2735, Sep. 2010.
[20] R. M. Nguimdo, Y. K. Chembo, P. Colet and L. Larger, "On the phase noise performance of nonlinear double-loop optoelectronic microwave oscillators," *IEEE J. Quantum Electron.*, vol. 48, no. 11, pp. 1415–1423, Nov. 2012.
[21] R. M. Nguimdo, K. Saleh, A. Coillet, G. Lin, R. Martinenghi, and Y. K. Chembo, "Phase noise performance of optoelectronic oscillators based on whispering-gallery mode resonators," *IEEE J. Quantum Electron.*, vol. 51, no. 11, pp. 1–8, Nov. 2015.
[22] A. Matsko, A. Savchenkov, D. Strekalov, V. Ilchenko, and L. Maleki, "Review of applications of whispering-gallery mode resonators in photonics and nonlinear optics," *IPN Prog. Rep.*, vol. 42, pp. 1–51, 2005.
[23] A. Chiasera *et al.*, "Spherical whispering-gallery-mode microresonators," *Laser Photon. Rev.*, vol. 4, 2010, Art. no. 457.
[24] D. V. Strekalov, C. Marquardt, A. B. Matsko, H. G. L. Schwefel and G. Leuchs, "Nonlinear and quantum optics with whispering gallery resonators," *J. Opt.*, vol. 18, 2016, Art. no. 123002.
[25] A. Coillet *et al.*, "Microwave photonics systems based on whispering-gallery-mode resonators," *J. Vis. Exp.*, vol. 78, 2013, Paper e50423.
[26] G. Lin, A. Coillet, and Y. K. Chembo, "Nonlinear photonics with high-q whispering-gallery-mode resonators," *Adv. Opt. Phot.*, vol. 9, 2017, Art. no. 828.
[27] P. Rabiei, W. H. Steier, C. Zhang, and L. R. Dalton, "Polymer micro-ring filters and modulators," *J. Lightw. Technol.*, vol. 20, no. 11, pp. 1968–1975, Nov. 2002.
[28] N. G. Pavlov, N. M. Kondratyev, and M. L. Gorodetsky, "Modeling the whispering gallery microresonator-based optical modulator," *Appl. Opt.*, vol. 54, 2015, Art. no. 10460.
[29] Y. Ehrlichman, A. Khilo, and M. A. Popovic, "Optimal design of a microring cavity optical modulator for efficient RF-to-optical conversion," *Opt. Exp.*, vol. 26, 2018, Art. no. 2462.
[30] A. Parriaux, K. Hammani, and G. Millot, "Electro-optic frequency combs," *Adv. Opt. Photon.*, vol. 12, 2020, Art. no. 223.
[31] V. S. Ilchenko, A. A. Savchenkov, A. B. Matsko, and L. Maleki, "Whispering-gallery-mode electro-optic modulator and photonic microwave receiver," *J. Opt. Soc. Amer. B.*, vol. 20, 2003, Art. no. 333.
[32] D. A. Cohen and A. F. J. Levi, "Microphotonic millimetre-wave receiver architecture," *Electron. Lett.*, vol. 37, pp. 37–39, 2001.
[33] V. S. Ilchenko, A. A. Savchenkov, A. B. Matsko, and L. Maleki, "Sub-microwatt photonic microwave receiver," *IEEE Photon. Technol., Lett.* vol. 14, no. 11, pp. 1602–1604, Nov. 2002.
[34] M. Hossein-Zadeh and A. F. J. Levi, "14.6-GHz $LiNbO_3$ microdisk photonic self-homodyne RF receiver," *IEEE Trans. Microw. Theory Techn.*, vol. 54, no. 2, pp. 821–831, Feb. 2006.
[35] V. S. Ilchenko, A. B. Matsko, I. Solomatine, A. A. Savchenkov, D. Seidel, and L. Maleki, "Ka-band all-resonant photonic microwave receiver," *IEEE Photon. Technol. Lett.*, vol. 20, no. 19, pp. 1600–1612, Oct. 2008.
[36] A. B. Matsko, D. V. Strekalov, and N. Yu, "Sensitivity of terahertz photonic receivers," *Phys. Rev. A.*, vol. 77, 2008, Art. no. 043812.
[37] D. V. Strekalov, A. A. Savchenkov, A. B. Matsko, and N. Yu, "Efficient upconversion of subterahertz radiation in a high-q whispering gallery resonator," *Opt. Lett.*, vol. 34, 2009, Art. no. 713.
[38] D. V. Strekalov, H. G. L. Schwefel, A. A. Savchenkov, A. B. Matsko, L. J. Wang, and N. Yu, "Microwave whispering-gallery resonator for efficient optical up-conversion," *Phys. Rev. A.*, vol. 80, 2009, Art. no. 033810.
[39] A. A. Savchenkov, A. B. Matsko, W. Liang, V. S. Ilchenko, D. Seidel, and L. Maleki, "Single-sideband electro-optical modulator and tunable microwave photonic receiver," *IEEE Trans. Microw. Theory Techn.*, vol. 58, no. 11, pp. 3167–3174, Nov. 2010.
[40] G. S. Botello *et al.*, "Sensitivity limits of millimeter-wave photonic radiometers based on efficient electro-optic upconverters," *Optica*, vol. 5, 2018, Art. no. 1210.
[41] Y. K. Chembo, "Quantum dynamics of kerr optical frequency combs below and above threshold: Spontaneous four-wave mixing, entanglement, and squeezed states of light," *Phys. Rev. A.*, vol. 93, 2016, Art. no. 033820.
[42] R. Toral and P. Colet, *Stochastic Numerical Methods*. Hoboken, NJ, USA: Wiley, 2014.
[43] A. H. Nayfeh, *The Method of Normal Forms*. Hoboken, NJ, USA: Wiley, 2011.